Multifunctional Nanoparticles with Superparamagnetic Mn(II) Ferrite and Luminescent Gold Nanoclusters for Multimodal Imaging

Barbara Casteleiro , Mariana Rocha , Ana R. Sousa , André M. Pereira , José M.G. Martinho * , Clara R. Pereira , José P. S. Farinha *

Posted Date: 2 October 2023

doi: 10.20944/preprints202310.0032.v1

Keywords: Gold nanoclusters; manganese ferrite nanoparticles; mesoporous silica; multimodal imaging; NIR-photoluminescence; superparamagnetism.

Article

Multifunctional Nanoparticles with Superparamagnetic Mn(II) Ferrite and Luminescent Gold Nanoclusters for Multimodal Imaging

Bárbara Casteleiro [a,b], Mariana Rocha [b,1], Ana R. Sousa [b,c], André M. Pereira [c], José M. G. Martinho [a,*], Clara Pereira [b,*] and José P.S. Farinha [a,*]

[a] Centro de Química Estrutural, Instituto de Ciências Moleculares (IMS), Departamento de Engenharia Química, Instituto Superior Técnico, Universidade de Lisboa, 1049-001 Lisboa, Portugal
[b] REQUIMTE/LAQV, Departamento de Química e Bioquímica, Faculdade de Ciências, Universidade do Porto, Rua do Campo Alegre s/n, 4169-007, Porto, Portugal
[c] IFIMUP - Instituto de Física de Materiais Avançados, Nanotecnologia e Fotónica, Departamento de Física e Astronomia, Faculdade de Ciências, Universidade do Porto, Rua do Campo Alegre s/n, 4169-007, Porto, Portugal
* Correspondence: jgmartinho@tecnico.ulisboa.pt; farinha@tecnico.ulisboa.pt; clara.pereira@fc.up.pt

Abstract: Gold nanoclusters (AuNCs) with fluorescence in the Near Infrared (NIR) by both one- and two-photon electronic excitation were incorporated in mesoporous silica nanoparticles (MSNs) using a novel one-pot synthesis procedure where the condensation polymerization of alkoxysilane monomers in the presence of the AuNCs and a surfactant produce hybrid MSNs of 49 nm diameter. This method was further developed to prepare 30 nm diameter nanocomposite particles with simultaneous NIR fluorescence and superparamagnetic properties, with a core composed of superparamagnetic manganese ferrite nanoparticles ($MnFe_2O_4$) coated with a thin silica layer, and a shell of mesoporous silica decorated with AuNCs. The nanocomposite particles feature NIR-photoluminescence with 0.6% quantum yield and large Stokes shift (290 nm), and superparamagnetic response at 300 K, with a saturation magnetization of 13.4 emu g^{-1}. The conjugation of NIR photoluminescence and superparamagnetic properties in the biocompatible nanocomposite has high potential for application in multimodal bioimaging.

Keywords: gold nanoclusters; manganese ferrite nanoparticles; mesoporous silica; multimodal imaging; NIR-photoluminescence; superparamagnetism

1. Introduction

Gold nanoclusters (AuNCs), with diameters below 2 nm, have been attracting a growing interest as probes for optical imaging. Unlike larger gold nanoparticles (AuNPs), with diameters above 2 nm, AuNCs have no surface plasmon resonance (SPR),[1] however they feature size-dependent photoluminescence, large Stokes shift, high photostability and biocompatibility.[2-6] These characteristics make them excellent candidates for photoluminescence-based imaging.[7]

Incorporation of AuNCs in multifunctional nanostructures combining photoluminescence and magnetic properties open new opportunities for developing dual bioimaging applications, combining optical imaging and magnetic resonance imaging (MRI).[7-10] To improve MRI contrast in soft tissues, contrast agents are commonly employed, with superparamagnetic transition metal ferrite nanoparticles (iron oxides) already being medically approved.[11,12] The use of superparamagnetic nanoparticles, as opposed to ferromagnetic materials, is important to avoid particles aggregation.

[1] Current affiliation: IFIMUP - Instituto de Física de Materiais Avançados, Nanotecnologia e Fotónica, Departamento de Física e Astronomia, Faculdade de Ciências, Universidade do Porto, Rua do Campo Alegre s/n, 4169-007, Porto, Portugal.

 doi:10.20944/preprints202310.0032.v1

Transition metal ferrite nanoparticles (MFe_2O_4, with M(II) being a 3*d* transition metal cation) have high potential as MRI contrast agents due to their high saturation magnetization, easy preparation, and superparamagnetic behavior at room temperature below a certain particle size.[10,13] These typically lead to negative contrast enhancement (T_2-type contrast agents).[14] Special emphasis has been put on the manganese ferrite $MnFe_2O_4$ because of its good colloidal stability, and very high saturation magnetization values within the transition metal ferrites family.[15-18]

While the conjugation of larger AuNPs and MFe_2O_4 nanoparticles has been widely explored in the field of catalysis[13,19-24] and multimodal imaging,[25-28] the conjugation of the magnetic nanoparticles with luminescent AuNCs,[29-34] shows remarkable potential for multimodal bioimaging[31-33] and sensing.[35,36]

One of the main drawbacks of most nanoparticles for multimodal systems is the lack of colloidal stability under demanding environments, such as the biological media. One strategy to overcome the poor colloidal stability of AuNCs and bare ferrite nanoparticles is to use an encapsulating matrix. Among different possibilities, the condensation polymerization of alkoxysilane monomers to produce a silica matrix, offers excellent opportunities for the stabilization of nanoparticles and further functionalization of the nanocomposites without affecting their properties. In the case of transition metal ferrites, the silica shell provides protection against dissolution and redox reactions in harsh media, and facilitates the conjugation with other species without interfering with the superparamagnetic behavior.[13] Silica can be prepared by simple and cost-effective routes, with good control over morphology and porosity, good colloidal stability, biodegradability and bioclearance, as well as huge flexibility for surface modification.[37-39] Mesoporous silica nanoparticles (MSNs) are specially promising, due to their large surface area, simple functionalization and tunable pore size.[40-45] These have been widely used in the encapsulation of different inorganic nanoparticles, such as quantum dots, carbon nanomaterials, gold nanoparticles and iron oxides.[45] In the case of AuNCs, the encapsulation into MSNs have been mostly for application in catalysis.[46-49] Among the few examples for optical applications, AuNCs have been incorporated into a mesoporous silica shell coating Nd^{3+}-sensitized up-conversion nanoparticles, for light-Induced imaging-guided multifunctional cancer therapy .[50]

One reason the incorporation of AuNCs into MSNs have not been more explored is the incompatibility between the commonly used silica precursors and AuNCs.[46-48] Here, we report the encapsulation of (3-mercaptopropyl)trimethoxysilane stabilized AuNCs (MPTS-AuNCs) in MSNs of 49 ± 8 nm diameter by a one-pot synthesis. This new approach allows to encapsulate the AuNCs in the silica matrix, bypassing the issues due to the incompatibility between the AuNCs precursors and the silica surface. This approach was further used to prepare composite nanoparticles with a $MnFe_2O_4$ superparamagnetic core, coated with a thin layer of dense silica, and a mesoporous silica shell containing MPTS-AuNCs. The hybrid nanocomposite (26 ± 5 nm in diameter), features NIR emission and superparamagnetic behavior at room temperature, with a saturation magnetization of 13.4 emu g^{-1} at 300 K. The bimodal nanoparticles are prepared through green chemistry, in a simple procedure that encapsulates AuNCs and $MnFe_2O_4$ in silica without extra functionalization or ligand exchange steps.

2. Materials and Methods

2.1. Materials and reagents

Hydrogen tetrachloroaurate(III) hydrate ($HAuCl_4 \cdot 3H_2O$, ≥99.9% trace metals basis, Sigma-Aldrich), (3-mercaptopropyl)trimethoxysilane (MPTS, 95%, Sigma-Aldrich), sodium hydroxide (NaOH, pure, EKA pellets) and sodium borohydride ($NaBH_4$, >98.5%, Sigma-Aldrich) were used as received in the synthesis of MPTS-AuNCs in ultra-pure water, from a Millipore Milli-Q system (resistivity ≥18 MΩ cm, Merck). Absolute ethanol (99.9%, Scharlau), *N*-cetyltrimethylammonium bromide (CTAB, 99%, Sigma-Aldrich), tetraethyl orthosilicate (TEOS, 99%, Sigma-Aldrich) were used in the synthesis of the mesoporous nanoparticles (MSNs). 1-amino-2-propanol (MIPA, 93%, Aldrich), Mn(II) chloride tetrahydrate ($MnCl_2 \cdot 4H_2O$, 99%, Merck), Fe(III) chloride hexahydrate ($FeCl_3.6H_2O$,

 doi:10.20944/preprints202310.0032.v1

98%, Riedel-de Haën) and hydrochloric acid (37%, analytical grade, Panreac) were used in the synthesis of the $MnFe_2O_4$ nanoparticles. Aqueous ammonia solution (NH_4OH, 28%, VWR) and triethylamine (TEA, ≥99.5%, Sigma-Aldrich) were used for the fabrication of the dense and mesoporous SiO_2 shells, respectively. All reagents were used without further purification.

2.2. Synthesis of (3-mercaptopropyl)trimethoxysilane stabilized AuNCs (MPTS-AuNCs)

5 mL of a 17.1 mM aqueous solution of $HAuCl_4 \cdot 3H_2O$ were stirred at 30 °C under magnetic stirring. 32.5 µL of MPTS were added to the solution. Finally, 100.5 µL of $NaBH_4$ solution (0.11 M at 0 °C) were added dropwise. The reaction mixture was left under stirring for 5 min at 30 °C, quickly changing from yellow to light brown color. The dispersion was used without further purification or dilution.

2.3. One-pot synthesis of MPTS-AuNCs in MSNs (MPTS-AuNCs@MSN)

The MSNs were synthesized by a modified sol–gel process,[43] adapted to simultaneously incorporate the MPTS-AuNCs. In a 500 mL polypropylene flask, 47 mL of Millipore water, 0.100 g of CTAB and 350 µL of 1.08 M NaOH aqueous solution were stirred at 30 °C. 1 mL of a solution of 0.13 M $HAuCl_4 \cdot 3H_2O$ was added to the mixture, forming an orange precipitate. 175 µL of 1.08 M NaOH were added to adjust the pH to 10, and the dispersion was stirred for 2 h until the precipitate was no longer present, and a homogeneous yellow dispersion was achieved. 50.5 µL of MPTS were added, leading to the change of the color of the dispersion from yellow to white. In a last step, 719 µL of $NaBH_4$ solution (0.01 M in 0.22 M NaOH) were added dropwise, followed by the dropwise addition of 450 µL of TEOS. The dispersion was left stirring for 3 h at 30 °C. The final nanomaterial (MPTS-AuNCs@MSN) was purified by 4 cycles of washing with ethanol and centrifugation, being stored at room temperature in ethanol. CTAB was removed by sonication of the MPTS-AuNCs@MSN (300 mg), previously dried under vacuum, in 15 mL of 0.5 M HCl in ethanol.

2.4. Preparation of $MnFe_2O_4$ magnetic nanoparticles ($MnFe_2O_4$ NPs)

The $MnFe_2O_4$ nanoparticles were prepared by a coprecipitation methodology previously developed by Pereira *et al.*[51] 10 mmol of $MnCl_2 \cdot H_2O$ were dissolved in 5 mL of an aqueous solution of HCl (2.4 M) and 20 mmol $FeCl_3.6H_2O$ were dissolved in 40 mL of water. The solutions were heated to 50 °C and quickly mixed with 200 mL of 3.0 M aqueous solution of MIPA at 100 °C. The reaction was kept under vigorous mechanical stirring for 2 h at 100 °C. The resulting material, denoted as $MnFe_2O_4$, was magnetically separated, washed with water, and stored at room temperature in aqueous medium.

2.5. Silica coating of $MnFe_2O_4$ magnetic nanoparticles ($Mn@SiO_2$)

319 µL of $MnFe_2O_4$ nanoparticles dispersion in water (21.3 g/L, $MnFe_2O_4$) were added to 80 mL of ethanol, followed by sonication during 30 min. Then 1.2 mL NH_4OH solution (28%) were added, followed by the dropwise addition of 8 mL of 0.03 M TEOS in ethanol. The reaction was left stirring at room temperature for 3 h. The resulting material, denoted as $Mn@SiO_2$, was washed with ethanol, and dried under vacuum.

2.6. Hybrid nanocomposite conjugating $Mn@SiO_2$ and MPTS-AuNCs (Mn@SiO2@AuNCs)

20 mg of $Mn@SiO_2$ were dispersed in 7.3 mL of water. 2.60 mL of 0.075 M CTAB aqueous solution were added to the dispersion, which was stirred for 10 min at 60 °C. Then, 0.2 mL of TEA were added to the dispersion. A solution of 114 µL TEOS and 1.16 mL of MPTS-AuNCs (TEOS:MPTS = 6.7 (n/n)) were added dropwise to the $Mn@SiO_2$ dispersion and the resulting mixture was stirred for 2h30 at 60 °C. The final material, named Mn@SiO2@AuNCs, was washed with ethanol and dried. CTAB was removed by multiple washes with an ethanolic solution of ammonium nitrate at reflux temperature for 2 h. The characterization was performed after purification of the Mn@SiO2@AuNCs, ensuring that the silica, CTAB or AuNCs that were not incorporated in the $Mn@SiO_2$ NPs, were removed.

 doi:10.20944/preprints202310.0032.v1

2.7. Characterization of the materials

Transmission Electron Microscopy (TEM). The TEM images were acquired with two microscopes. The first one was a Hitachi transmission electron microscope (Hitachi, model H-8100, Tokyo, Japan), operating at an acceleration voltage of 200 kV, with the images being acquired by the camera KeenView of Soft Imaging System, using the software iTEM. The second TEM equipment was a JEOL JEM 1400 microscope, operating at an acceleration voltage of 120 kV and equipped with a charge-coupled device (CCD) digital camera Orious (1100 W). The samples were prepared by direct deposition of 10 μL of the dispersion in a carbon-coated 400 mesh copper grid, followed by drying at room temperature.

Scanning Electron Microscopy. Energy Dispersive X-ray Spectroscopy (SEM - EDS). The SEM images were obtained on a FEG-SEM JEOL JSM7001F equipment at 15.0 kV coupled with an EDS Inca 250 Oxford light elements detector. The samples were coated with chromium (Cr).

Confocal Microscopy and Two-photon Measurements. Confocal images were obtained on a Leica TCS SP5 (Leica Microsystems CMS GmbH, Manheim, Germany) inverted confocal microscope (DMI600). Excitation lines provided by an Argon ion laser or a He-Ne laser were focused into the sample by an apochromatic water immersion objective (63x, NA 1.2; Zeiss, Jena Germany). A 111.4 μm diameter pinhole positioned in front of the image plane blocked out-of-focus signals. Two-photon excitation measurements of AuNCs were obtained using the same set-up coupled to a Ti:sapphire laser (Mai Tai, Spectra-Physics, Darmstadt, Germany) as the excitation source (wavelength range 710-990 nm, 1.7W, 100 fs, 82 MHz).

Fourier Transform Infrared (FTIR). The FTIR spectra were recorded on a Jasco FT/IR-460 Plus spectrophotometer in the 400–4000 cm^{-1} range, at room temperature, with a resolution of 4 cm^{-1} and 32 scans. The spectra of the samples were obtained using KBr pellets (Aldrich, FTIR spectroscopy grade) containing 1 wt% of the nanomaterials.

Dynamic Light Scattering (DLS). The hydrodynamic diameter of the nanomaterials was measured with a Zetasizer Nano ZS apparatus (Malvern Instruments, UK) using laser light of 633 nm and recording the scattered light at the scattering angle of 173°.

Atomic Absorption Spectroscopy (AAS). AAS was performed using a Philips PU 9200X device equipped with a hollow cathode lamp (S & J Juniper & Co) to determine the concentration of the $MnFe_2O_4$ aqueous dispersion and Mn:Fe ratio. The samples were prepared by digesting $MnFe_2O_4$ aqueous dispersion with concentrated HCl (12 M). The mixture was stirred at 40 °C at room temperature overnight.

Superconducting Quantum Interference Device (SQUID). SQUID magnetometry was used to determine the magnetic properties of the samples containing $MnFe_2O_4$ nanoparticles using Quantum Design's MPMS 3 equipment. The measurements of the magnetization as a function of the applied magnetic field ($M(H)$) were performed at 300 and 5 K for a maximum applied magnetic field of 50 kOe. Temperature-dependent zero-field-cooled (ZFC) and field-cooled (FC) measurements were performed over the temperature range of 5–300 K with an applied magnetic field of 100 Oe.

UV-vis Absorption Spectroscopy. The UV-vis absorption spectra of the samples containing AuNCs were acquired on a Jasco UV-660 spectrophotometer (Jasco International, Tokyo) with a Peltier temperature controller cuvette holder (Jasco International, Tokyo).

Steady State Photoluminescence. The photoluminescence spectra of the samples containing AuNCs were recorded on a Fluorolog 3-22 spectrofluorimeter (Horiba Jobin Yvon, USA) equipped with a 450 W xenon lamp. The fluorescence quantum yields (Φ) were determined by the reference method using a 5,10,15,20-tetraphenyl-21*H*,23*H*-porphyrin (TPP) solution in toluene (0.24 mM; Φ = 11 %, λ_{exc} (excitation wavelength) = 510; 575 nm< λ_{em} (emission wavelength) < 850 nm) as the standard.[52] The quantum yield (Φ) was calculated as $\Phi_{sample} = \Phi_{TPP}\left(slope_{sample}/slope_{TPP}\right)\left(n^2_{sample}/n^2_{TPP}\right)$, where the slopes correspond to the linear correlation between the integrated emission spectra with λ_{exc} = 510 nm and the absorbance at λ = 510 nm (refractive index n of toluene and water equal to 1.50 and 1.33, respectively).

Preprints (www.preprints.org) | NOT PEER-REVIEWED | Posted: 2 October 2023 doi:10.20944/preprints202310.0032.v1

3. Results and discussion

We prepared mesoporous silica nanoparticles (MSNs) with dual imaging capabilities, incorporating photoluminescent gold nanoclusters (AuNCs) and superparamagnetic manganese ferrite ($MnFe_2O_4$) nanoparticles. We start by developing a one-pot synthesis of MSNs incorporating AuNCs stabilized with (3-mercaptopropyl)trimethoxysilane (AuNCs@MSN) that overcomes the incompatibility between usual preparation procedures. This was then used to develop a green encapsulation strategy for both AuNCs and $MnFe_2O_4$ nanoparticles in MSNs, without further functionalization or ligand exchange steps.

3.1. Synthesis and characterization of AuNCs stabilized with MPTS

The synthesis of MPTS- stabilized AuNCs was performed in ethanol at 30°C, following the Brust one-phase method.[53] The Au(III) salt was solubilized in ethanol and mixed with MPTS, leading to the partial reduction of Au(III) to Au(I) induced by MPTS.[54] An aqueous solution of $NaBH_4$ at 0°C was added right after, leading to the further reduction of Au(I) to Au(0) and formation of MPTS-AuNCs. The reduction of the gold salt under mild conditions allows a better control over the AuNCs growth. The formation of AuNCs can be observed by the evolution of the color of the dispersion from yellow to brown (**Figure S1A** in Supporting Information). The dispersion became turbid over time, due to the hydrolysis and condensation of the methoxy groups of MPTS to form silica oligomers.

Figure 1 shows the photoluminescence spectrum of a MPTS-AuNCs dispersion in ethanol, featuring a broad band with maximum in the NIR (λ_{em}^{max} = 715 nm), as well as the excitation spectrum recorded at λ_{em} = 675 nm (maximum intensity at λ_{exc}^{max} = 425 nm) corresponding to the photoluminescence of the AuNCs (**Figure S1B** in Supporting Information).

The UV-vis absorption spectrum of the MPTS-AuNCs dispersion in ethanol shows a slight shoulder at λ = 550 nm, corresponding to the surface plasmon resonance (SPR) of a small amount of AuNPs (with diameter above 2 nm) that are formed during the synthesis (**Figure 1**). The Stokes shift is 290 nm (no overlap of emission and absorption), and the photoluminescence quantum yield is Φ = 0.6% (calculated using TPP in toluene as standard, with excitation at λ_{exc} = 510 nm). The photoluminescence quantum yield is slightly higher than the value previously reported for AuNCs stabilized with small thiol molecules.[55-57]

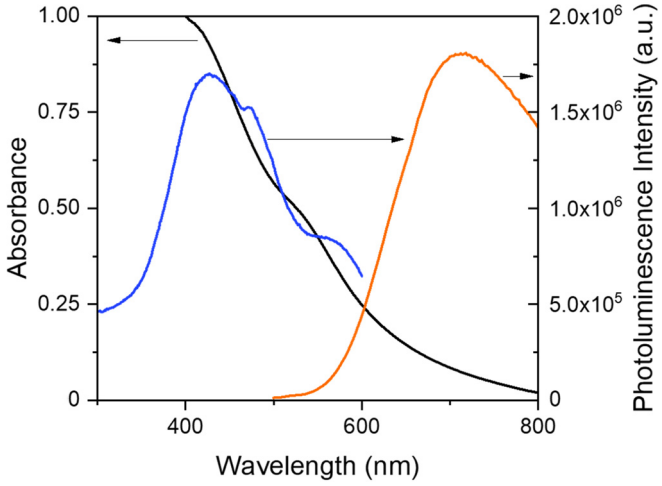

Figure 1. Linear optical properties of an AuNCs dispersion in ethanol (black: absorption spectrum; blue: photoluminescence excitation spectrum, λ_{em} = 675 nm; orange: photoluminescence emission spectrum, λ_{exc} = 450 nm).

3.2. One-pot synthesis of AuNC in MSN (AuNCs@MSN)

The synthesis of the AuNCs@MSN was developed by coupling the synthesis of MPTS-stabilized AuNCs with the typical preparation method of MSNs, in water using CTAB as template and TEOS

Preprints (www.preprints.org) | NOT PEER-REVIEWED | Posted: 2 October 2023 doi:10.20944/preprints202310.0032.v1

as silica precursor.[37] MPTS is a thiol-terminated organosilane, which allows the stabilization of the AuNCs with the thiol group and the incorporation of the AuNCs directly into the silica matrix through the methoxy groups. This approach overcomes the limitations previously reported in the literature, relative to the incompatibility of the silica surface with the Au(III) salt, without requiring extra steps of surface functionalization or ligand exchange.[46-48]

The synthesis was performed in alkaline aqueous medium at 30 °C in the presence of the silica precursor. First, the Au(III) aqueous solution was added to a basic CTAB solution, producing an orange precipitate due to the complexation of $HAuCl_4$ with CTAB.[58] The pH was adjusted to 10 using a 1.08 M NaOH aqueous solution. After strong stirring for 1 h, the orange precipitate was dispersed, originating a yellow solution. After 3 h, MPTS was added to the dispersion that turned transparent due to the formation of Au(I)-MPTS complexes by the partial reduction of Au(III) to Au(I) by the thiol group of MPTS.[54] The Au reduction was completed by dropwise addition of a solution of $NaBH_4$ resulting in the color change to brown, expected for the MPTS-stabilized AuNCs. Immediately after, TEOS was added dropwise to form the AuNCs incorporated in MSNs (AuNCs@MSN), which increased the turbidity and led to flocculation of the particles (and their deposition at the bottom in the absence of stirring). This approach overcomes the difficulties previously reported for the encapsulation of AuNCs in MSNs,[49] allowing the one-pot green synthesis of the nanocomposite. The AuNCs@MSN nanoparticles were then washed with ethanol and the CTAB template was removed by a HCl solution in ethanol.

Before purification the AuNCs@MSN hybrid particles have an average hydrodynamic diameter of 75 ± 9 nm in water (measured by DLS). However, the DLS intensity autocorrelation curve shows a noisy baseline (**Figure S2** in Supporting Information), suggesting the sedimentation of AuNCs@MSN over time. Both the TEM and SEM images show that the AuNCs@MSN present an irregular shape, which can be attributed to the presence of the Au(III) salt before the formation of the MSNs (**Figure 2A and S3A** in Supporting Information).[59] The TEM images show that the AuNCs have an average diameter of 1.3 ± 0.2 nm and are embedded in the silica structure (**Figure 2A**). The SEM images taken after AuNCs@MSN purification to remove salts and free Au particles/complexes (**Figure S3A** in Supporting Information), yield an average AuNCs@MSN diameter of 49 ± 8 nm (**Figure S3B** in Supporting Information). EDS-SEM confirms the presence of Au structures in the silica matrix (**Figure S3C** in Supporting Information). The presence of chromium is a contamination arising from coating the sample for SEM measurements.

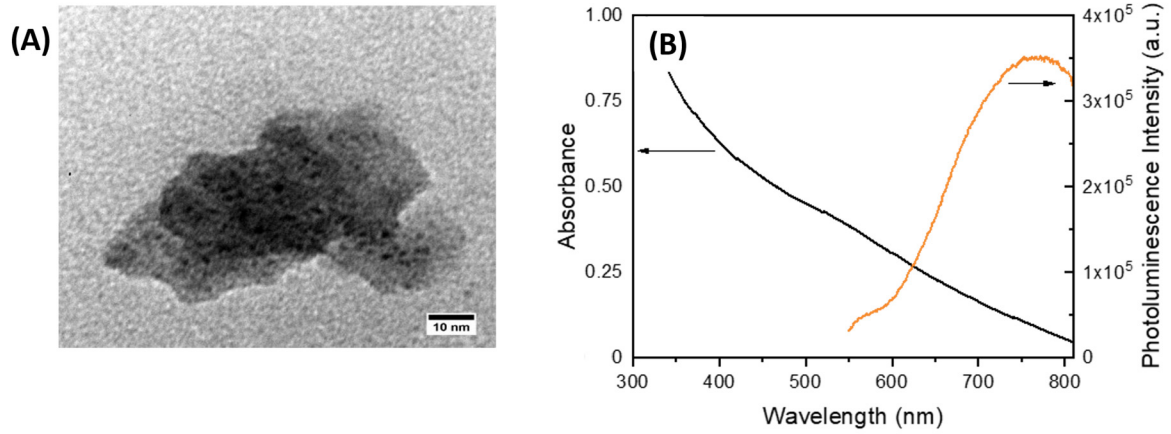

Figure 2. Characterization of AuNC@MSN: (A) TEM image (magnification: 800 000×). (B) Linear optical properties in water (black: absorption; orange: photoluminescence emission spectrum, λ_{exc} = 300 nm).

The UV-vis absorption spectrum of the AuNCs@MSN dispersion in water (**Figure 2B**) shows a slight shoulder at λ = 550 nm due to the surface plasmon resonance (SPR) of AuNPs (with diameter above 2 nm) present in trace amounts (also observed for the MPTS-stabilized AuNCs described above). Upon excitation at 300 nm, a photoluminescence emission band in the NIR (λ_{em}^{max}= 750 nm),

characteristic of AuNCs, is observed (**Figure 2B** and **Figure S4A** in Supporting Information). The small red shift in the emission, compared to that observed for individual AuNCs in ethanol (**Figure 1**), can be attributed to the change in the AuNCs environment (silica and water), since the AuNC@MSN are dispersed in water.

Laser excitation at 900 nm shows a quadratic dependence of the photoluminescence intensity on the excitation power, indicating that a two-photon absorption occurred (Figure S4B in Supporting Information). The silica-encapsulated AuNCs can thus be electronically excited by two-photon absorption in the NIR, which is very useful for imaging of biological samples (Figure S4C and D in Supporting Information).

To better control the formation of the AuNC and MSNs, the pH was adjusted to 10 (by addition of NaOH) during both the preparation of the starting solution containing CTAB and Au(III), and the TEOS addition to form the MSNs (instead of only during the preparation of the CTAB/Au(III) solution). The NIR photoluminescence emission of the AuNCs remained, while the formation of the larger AuNPs (d > 2 nm) was suppressed, with the SPR band disappearing from the absorption spectrum of the AuNCs@MSN (**Figure S5** in the Supporting Information).

The influence of temperature on the morphology and photoluminescent properties of the nanomaterials was evaluated by changing the preparation temperature from 30°C to 35°C and 65°C, while keeping pH 10 in the CTAB and Au(III) solutions. At 30°C, AuNC@MSN with irregular morphology are formed (**Figure 2A**), while at 35 °C silica rods are formed (**Figure S6A** in Supporting Information), and at 65 °C a mixture of worm-like and spherical particles are obtained (**Figure S6B** in the Supporting Information). The presence of AuNPs (d > 2 nm) is more apparent in the UV-vis absorption spectra pf the particles prepared at higher temperatures (**Figure S6C** in Supporting Information). The photoluminescence of the AuNC@MSN is slightly broadened and blue-shifted with the increase in temperature (**Figure S6D** in Supporting Information).

In conclusion, the best reaction temperature is 30 °C, since it is high enough for the solubilization of CTAB and the formation of the template for the mesoporous structure, while maintaining the optical properties of the resulting AuNCs. On the other hand, the addition of NaOH during the different steps of the synthesis, as opposite to the addition of NaOH only to the CTAB and Au(III) solution, seems to avoid the formation of AuNPs at lower temperature.

3.3. Incorporation of AuNCs and $MnFe_2O_4$ in MSNs

Magnetic nanoparticles were synthesized by coprecipitation, and their composition was determined by atomic absorption spectroscopy as $MnFe_{2.6}O_4$. The TEM images show nearly spherical particles with an average diameter of 13 ± 3 nm (**Figure S7** in Supporting Information), similar to the results described in the literature.[51]

To increase the colloidal stability and protect the nanoparticles, they were coated with a thin dense silica shell ($Mn@SiO_2$). The core-shell nanoparticles have an average diameter of 15 ± 3 nm (by TEM), with their morphology unchanged (**Figures S8A and B** in Supporting Information). FTIR measurements (**Figure S8C** in the Supporting Information) shows that the band at 582 cm^{-1} (Fe–O and Mn–O stretching vibrations of the transition metal ferrite) is present before and after encapsulation with the silica shell. The presence of silica is confirmed by the bands at 1086 cm^{-1} with a shoulder around 1200 cm^{-1} (Si–O–Si asymmetric stretching), at 950 cm^{-1} (Si-OH stretching), 800 cm^{-1} (Si–O–Si symmetric stretching) and 464 cm^{-1} (Si–O–Si rocking).[13,60,61]

Two possibilities were explored to conjugate the MPTS-stabilized AuNCs with the $Mn@SiO_2$ nanoparticles: (i) synthesis of the AuNCs simultaneously with a mesoporous silica shell (by addition of the gold salt to a dispersion containing $Mn@SiO_2$, NaOH and CTAB, followed by simultaneous addition of TEOS and MPTS); and (ii) *post*-grafting of previously obtained AuNCs (by addition of MPTS-stabilized AuNCs to a dispersion of $Mn@SiO_2$ in a solution of CTAB and NaOH, followed by the addition of TEOS). However, in both cases the nanocomposites (of size around 30 nm by TEM) do not show magnetic properties. This is probably due to the destruction by NaOH of the silica shell protecting the $MnFe_2O_4$.[62] The photoluminescence from the AuNCs in the Mn@SiO2@AuNC was also very low, without a well-defined emission band. Ammonia was then tested as an alternative

Preprints (www.preprints.org) | NOT PEER-REVIEWED | Posted: 2 October 2023 doi:10.20944/preprints202310.0032.v1

base, leading to nanocomposites with well-defined mesoporous structure and size around 35 ± 3 nm (by TEM), but without photoluminescence.

To avoid damaging the Mn@SiO_2 and the optical properties of the AuNCs, TEA was used as a mild base for the hydrolysis/condensation of the second layer of mesoporous silica. To accelerate the formation of the silica structure (decreasing the probability of AuNCs aggregation into AuNPs), the temperature was raised to 60 °C. In these conditions, a hybrid Mn@SiO2@AuNCs material was obtained independently of the step in which the AuNCs were added to the Mn@SiO_2, *i.e.*, both for *in situ* and *a priori* synthesis of the AuNCs (**Figure 3**). The addition of AuNCs to an aqueous dispersion of Mn@SiO_2 containing CTAB was performed in a second step after TEA addition, using TEOS as cross-linker between the two structures. The strategy based on *a priori* synthesis of the AuNCs in ethanol was found to lead to better control over the synthesis, minimizing the formation of plasmonic AuNPs (with d> 2 nm), and resulting in a more controlled preparation of the Mn@SiO2@AuNCs.

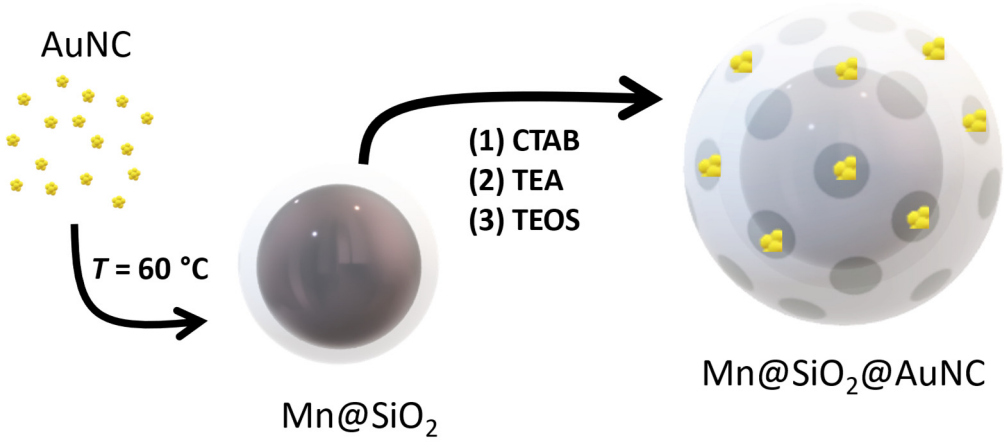

Figure 3. Schematics of the Mn@SiO2@AuNCs nanocomposite fabrication. The MPTS-AuNCs are synthesized in ethanol in a first step. Afterwards, they are mixed with Mn@SiO_2 NPs and CTAB in alkaline aqueous solution. This is followed by the addition of TEOS. TEA was used as base for the hydrolysis and condensation of MPTS-AuNCs and TEOS. The final nanocomposite consists of a core of $MnFe_2O_4$ with a mesoporous silica shell containing MPTS-AuNCs (Mn@SiO2@AuNC).

The TEM image of Mn@SiO2@AuNCs shows the encapsulation of Mn@SiO_2 in the mesoporous silica shell containing the AuNCs (**Figure 4A**). The particle size distribution determined by TEM (**Figure 4B)**, shows that the final particles have an average diameter of 26 ± 5 nm. EDS-SEM confirms the presence of AuNCs (Au and S), and $MnFe_2O_4$ (Mn and Fe) nanoparticles (**Figure S9** in the Supporting Information). The shell layer was also identified by the presence of Si (the O signal can be attributed both to the $MnFe_2O_4$ and SiO_2).

The synthesis of MSNs at T = 60°C using TEA as base, in the presence of AuNCs but with no Mn@SiO_2, leads to structures of 183 ± 55 nm in diameter by TEM. The dimensions are about 6-fold higher than those obtained in similar conditions but in the presence of Mn@SiO_2. The large dispersity in size and morphology shown by TEM (**Figure S10A** in the Supporting Information) indicates that the $MnFe_2O_4$ nanoparticles act as nucleation sites for the mesoporous silica formation, leading to smaller structures with lower size dispersity. Also, the synthesis of the mesoporous silica shell around the $MnFe_2O_4$ in the absence of AuNCs results in more coalesced structures (**Figure S10B** in the Supporting Information).

Figure 4C shows the photoluminescence emission and excitation spectra of the particles, confirming the NIR emission of the AuNCs. The reported absorption spectrum of $MnFe_2O_4$ [63] overlaps with the absorption spectrum of the AuNCs, and so the amount of excitation light absorbed by the AuNCs decreases in the presence of $MnFe_2O_4$, with a consequent decrease in the AuNCs photoluminescence intensity. Nevertheless, the photoluminescence spectra of Mn@SiO2@AuNCs in

Preprints (www.preprints.org) | NOT PEER-REVIEWED | Posted: 2 October 2023 doi:10.20944/preprints202310.0032.v1

water by excitation between 300 nm < λ_{exc} < 450 nm (**Figure S11** in the Supporting Information), are similar to those of isolated AuNCs in ethanol (**Figure S1** in the Supporting Information).

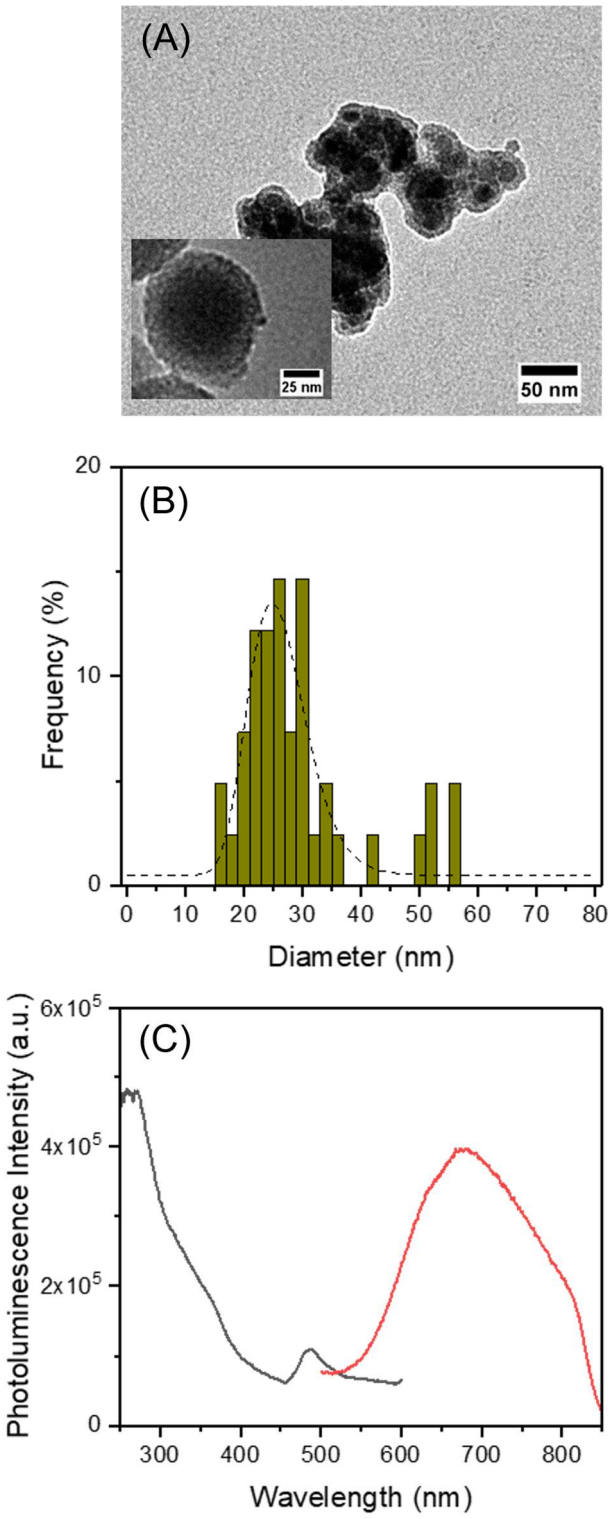

Figure 4. Characterization of Mn@SiO2@AuNCs: (A) TEM image (magnification: 150 000×, inset: 40 000×), (B) TEM particle size distribution histogram with log-normal fit (d = 26 nm; sigma = 5 nm; R^2 = 0.805).and (C) Linear optical properties in water (grey: photoluminescence excitation spectrum, λ_{em}=675 nm; red: photoluminescence emission spectrum, λ_{exc}=450 nm).

The isothermal magnetization measured as a function of the applied magnetic field at 300 K, for the samples containing $MnFe_2O_4$ (**Figure 5A**) show that all samples present negligible coercivity (H_c),

Preprints (www.preprints.org) | NOT PEER-REVIEWED | Posted: 2 October 2023 doi:10.20944/preprints202310.0032.v1

with coercive fields around 30 Oe (**Table 1**), a signature of superparamagnetic behavior. The saturation magnetization (M_S) values at 300 K decrease with the increase in the thickness of the silica shell, from 58.7 emu g^{-1} for $MnFe_2O_4$ to 30.1 emu g^{-1} for $Mn@SiO_2$, and 13.4 emu g^{-1} for Mn@SiO2@AuNCs. This decrease is attributed to the diamagnetic character of silica.[13] The presence of AuNCs seems to induce a slight increase in M_S, especially at 5 K (from 17.3 emu g^{-1} for $Mn@SiO_2$@MSN to 19.0 emu g^{-1} for Mn@SiO2@AuNCs). The presence of gold has been correlated with a reduction of the magnetic disordered regions, contributing to the spin alignment at the surface, in the case of AuNPs or of a gold shell.[64-67] The magnetic behavior of AuNCs is not consensual, with in-depth studies showing that it depends on their charge, structure, size and type of ligand.[68-70] Nevertheless, the AuNCs are generally considered to enhance the magnetic response of the system.

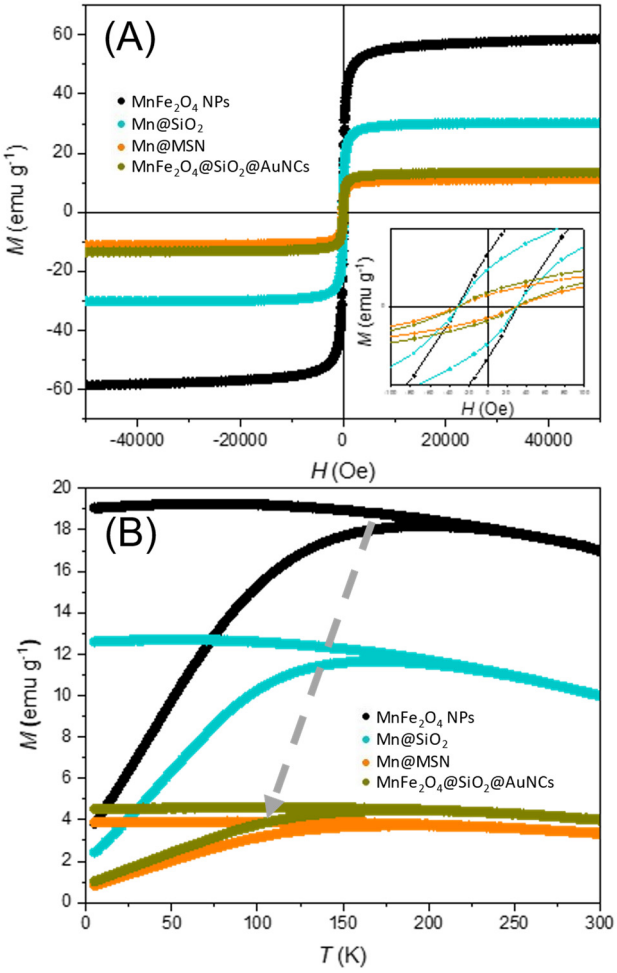

Figure 1. (A) $M(H)$ curves between -50 and 50 kOe at 300 K (black: $MnFe_2O_4$ NPs; blue: $Mn@SiO_2$; orange: $Mn@SiO_2$@MSN; gold: Mn@SiO2@AuNCs). (B) Temperature-dependence of the magnetization (ZFC and FC) over the temperature range of 5-300 K with H = 100 Oe (black: $MnFe_2O_4$ NPs; blue: $Mn@SiO_2$; orange: $Mn@SiO_2$@MSN; gold: Mn@SiO2@AuNCs). The grey arrow indicates the evolution of the convergence point between the ZFC (lower curve) and FC (top curve) curves ongoing from the uncoated $MnFe_2O_4$ NPs to the Mn@SiO2@AuNCs nanocomposite.

The zero-field-cooled (ZFC) and field-cooled (FC) curves for the samples containing $MnFe_2O_4$ (**Figure 5B**) converge at the so-called reversibility temperature (T_{rev}; see **Table 1**), which is lower than room temperature, indicating that the nanoparticles have superparamagnetic behavior at room temperature. However, it is not possible to estimate the blocking temperature (T_B, the temperature

Preprints (www.preprints.org) | NOT PEER-REVIEWED | Posted: 2 October 2023 doi:10.20944/preprints202310.0032.v1

below which the material shows ferromagnetic behavior) since the ZFC and FC curves tend to a plateau at higher temperatures for the different samples, suggesting that the dipolar interactions in $MnFe_2O_4$ are stronger than in other transition metal ferrites.[51] In the case of the silica-coated samples, the branching of the ZFC and FC curves occurs at lower temperatures (T_{rev}), especially in the presence of the mesoporous silica shell (**Table 1**), indicating a decrease in the dipolar interactions between the $MnFe_2O_4$ magnetic cores, as previously reported in the literature.[71]

Table 1. Magnetic properties of the $MnFe_2O_4$-based nanomaterials: saturation magnetization (M_S) at 5 K and 300 K; coercive field (H_C) at 300 K; reversibility temperature (T_{rev}).

Sample	M_S @ 5 K (emu/g)	M_S @ 300 K (emu/g)	H_C @ 300 K (Oe)	T_{rev} (K)
$MnFe_2O_4$	85.4	58.7	31.0	253
$Mn@SiO_2$	44.7	30.1	30.3	245
$Mn@SiO_2$@MSN	17.3	11.2	30.3	217
Mn@SiO2@AuNCs	19.0	13.4	30.2	241

The final nanocomposite shows better combined stability, magnetic and optical properties than previously reported multimodal materials, where AuNCs are combined with ferrites by electrostatic interactions, [32,33,72] or through silica layers.[36,73] H. Guo *et al.* developed a biocompatible water soluble iron-oxide gold nanocluster with the surface decorated with β-cyclodextrins (β-CD), Fe_3O_4@Au@β-CD, to diagnosis/therapy of gastric cancer cells.[32] AuNCs were previously stabilized with *L*-cysteine and showed photoluminescence emission at 600–700 nm. For comparison Fe_3O_4@Au@SiO_2 NPs were also prepared. The silica coated NPs show M_S = 7.41 emu g^{-1}, while the nanocomposite with β-CD exhibited M_S = 2.83 emu g^{-1} (room temperature). C. Wang *et al.* reported a system based on glutathione-stabilized AuNCs (GSH-AuNCs) and Fe_3O_4 nanoparticles for bioimaging.[33] The hydrophobic Fe_3O_4 nanoparticles were capped with CTAB to became hydrophilic and the nanocomposite was prepared by the adsorption of Fe_3O_4–CTAB nanoparticles on GSH–AuNCs through electrostatic attraction. The nanocomposite with average size of 13.5 nm has limited stability and featured emission at λ_{em} = 650 nm (with a Stokes shift of 120 nm), and M_S = 13.0 emu g^{-1} (room temperature). R. Huang *at al.* reported a similar system, using polyethyleneimine (PEI) instead of CTAB to combine GSH-AuNCs and Fe_3O_4 nanoparticles, for the visualization of latent fingerprints.[72] The nanocomposites with ~ 90 nm size, show M_S =29.2 emu g^{-1} (temperature not specified) and photoluminescence bands centered at 468 nm and 543 nm. The Fe_3O_4-PEI nanoparticles in the core quench the photoluminescence of the GSH-AuNCs in the shell of the nanocomposite. D. Kim *et al.* developed a core-shell nanocomposite, Fe_3O_4@SiO_2@AuNCs-MIP, with a Fe_3O_4 core, a silica shell with covalently bonded GSH-AuNCs and a molecular imprinted layer (MPI) formed by copolymerization, for detection of Bisphenol A.[36] The system presented M_S = 9.87 emu g^{-1} (temperature not specified) with photoluminescence emission band at 562 nm. The low value of the saturation magnetization of the nanocomposite was attributed to the reduction of the magnetic properties of Fe_3O_4 by the coating of silica and molecular imprinted polymers. X. Xiao et al. prepared multifunctional Fe_3O_4 nanoparticles coated with a mesoporous silica layer at which AuNCs where covalently bond for drug delivery[73]. The nanocomposite shows Ms = 24 emu g^{-1} , AuNCs emission at 630 nm and specific surface area of 27.8 m^2g^{-1}.

These reports show the potential of our multimodal probe for bioimaging, with high resistance and colloidal stability, and good optical and magnetic properties, one of the first using $MnFe_2O_4$ instead of Fe_3O_4 magnetic nanoparticles.

4. Conclusions

Our simple, one-pot, green synthesis of mesoporous silica nanoparticles containing photoluminescent AuNCs, uses water as solvent and mild conditions (T = 30 °C), overcoming the incompatibility between silica and the gold salt. The nanoparticles, with a diameter of 49 ± 8 nm, have good colloidal and optical stability over 5 months, featuring NIR emission and excellent potential for linear and non-linear photoluminescence imaging. This approach was adapted to obtain nanoparticles with both optical and magnetic response, combining a silica-coated superparamagnetic core of $MnFe_2O_4$ with a mesoporous silica shell containing the AuNCs. The preparation involves three steps: (i) synthesis of $MnFe_2O_4$ nanoparticles and coating with a thin silica shell ($Mn@SiO_2$), (ii) synthesis of NIR emitting MPTS-stabilized AuNCs, and (iii) conjugation of $Mn@SiO_2$ and AuNCs, using CTAB as template and TEOS as silica precursor. The resulting hybrid nanoparticles, with a 26 ± 5 nm diameter, maintain the NIR photoluminescence of the AuNPs and the magnetic properties with a saturation magnetization of 13.4 emu g^{-1} at 300 K, and superparamagnetic behavior at room temperature. The new nanocomposite shows great potential for multimodal imaging, with excellent optical and magnetic properties.

Acknowledgements: This work was supported by Fundação para a Ciência e a Tecnologia (FCT-Portugal) and COMPETE (FEDER) within projects PTDC/CTM-COM/1581/2021, UIDB/00100/2020, UIDP/00100/2020, UIDB/50006/2020, UIDP/50006/2020 and UIDB/04968/2020. BC also thanks FCT for PhD grant PD/BD/137511/2018. CP thanks FCT for funding through the Individual Call to Scientific Employment Stimulus (Ref. 2021.04120.CEECIND/CP1662/CT0008).

References

1. Piñeiro, Y.; Rivas, J.; López-Quintela, M. A.: Chapter 4 - The Emergence of Quantum Confinement in Atomic Quantum Clusters. In *Colloidal Foundations of Nanoscience*; Berti, D., Palazzo, G., Eds.; Elsevier: Amsterdam, 2014; pp 81-105.
2. Sahoo, A. K.; Banerjee, S.; Ghosh, S. S.; Chattopadhyay, A.: Simultaneous RGB Emitting Au Nanoclusters in Chitosan Nanoparticles for Anticancer Gene Theranostics. *ACS Applied Materials & Interfaces* **2014**, *6*, 712-724. 10.1021/am4051266
3. Chen, D.; Luo, Z.; Li, N.; Lee, J. Y.; Xie, J.; Lu, J.: Amphiphilic Polymeric Nanocarriers with Luminescent Gold Nanoclusters for Concurrent Bioimaging and Controlled Drug Release. *Adv. Funct. Mater.* **2013**, *23*, 4324-4331. 10.1002/adfm.201300411
4. Sun, Y.; Wang, D.; Zhao, Y.; Zhao, T.; Sun, H.; Li, X.; Wang, C.; Yang, B.; Lin, Q.: Polycation-functionalized gold nanodots with tunable near-infrared fluorescence for simultaneous gene delivery and cell imaging. *Nano Research* **2018**, *11*, 2392-2404. 10.1007/s12274-017-1860-4
5. Chen, Y.; Zheng, X.; Wang, X.; Wang, C.; Ding, Y.; Jiang, X.: Near-Infrared Emitting Gold Cluster–Poly(acrylic acid) Hybrid Nanogels. *ACS Macro Letters* **2014**, *3*, 74-76. 10.1021/mz4005748
6. Lin, C.-A. J.; Yang, T.-Y.; Lee, C.-H.; Huang, S. H.; Sperling, R. A.; Zanella, M.; Li, J. K.; Shen, J.-L.; Wang, H.-H.; Yeh, H.-I.; Parak, W. J.; Chang, W. H.: Synthesis, Characterization, and Bioconjugation of Fluorescent Gold Nanoclusters toward Biological Labeling Applications. *ACS Nano* **2009**, *3*, 395-401. 10.1021/nn800632j
7. Wu, X.; Li, C.; Liao, S.; Li, L.; Wang, T.; Su, Z.; Wang, C.; Zhao, J.; Sui, C.; Lin, J.: Silica-Encapsulated Gd3+-Aggregated Gold Nanoclusters for In Vitro and In Vivo Multimodal Cancer Imaging. *Chemistry – A European Journal* **2014**, *20*, 8876-8882. 10.1002/chem.201403202
8. Wu, X. T.; Li, L.; Zhang, L. Y.; Wang, T. T.; Wang, C. G.; Su, Z. M.: Multifunctional spherical gold nanocluster aggregate@polyacrylic acid@mesoporous silica nanoparticles for combined cancer dual-modal imaging and chemo-therapy. *Journal of Materials Chemistry B* **2015**, *3*, 2421-2425. 10.1039/c4tb02009j
9. Hembury, M.; Chiappini, C.; Bertazzo, S.; Kalber, T. L.; Drisko, G. L.; Ogunlade, O.; Walker-Samuel, S.; Krishna, K. S.; Jumeaux, C.; Beard, P.; Kumar, C.; Porter, A. E.; Lythgoe, M. F.; Boissiere, C.; Sanchez, C.; Stevens, M. M.: Gold-silica quantum rattles for multimodal imaging and therapy. *Proceedings of the National Academy of Sciences of the United States of America* **2015**, *112*, 1959-1964. 10.1073/pnas.1419622112
10. Shin, T.-H.; Choi, Y.; Kim, S.; Cheon, J.: Recent advances in magnetic nanoparticle-based multi-modal imaging. *Chemical Society Reviews* **2015**, *44*, 4501-4516. 10.1039/c4cs00345d

11. Wahsner, J.; Gale, E. M.; Rodríguez-Rodríguez, A.; Caravan, P.: Chemistry of MRI Contrast Agents: Current Challenges and New Frontiers. *Chemical Reviews* **2019**, *119*, 957-1057. 10.1021/acs.chemrev.8b00363
12. Xiao, Y.-D.; Paudel, R.; Liu, J.; Ma, C.; Zhang, Z.-S.; Zhou, S.-K.: MRI contrast agents: Classification and application (Review). *Int J Mol Med* **2016**, *38*, 1319-1326. 10.3892/ijmm.2016.2744
13. Rocha, M.; Fernandes, C.; Pereira, C.; Rebelo, S. L. H.; Pereira, M. F. R.; Freire, C.: Gold-supported magnetically recyclable nanocatalysts: a sustainable solution for the reduction of 4-nitrophenol in water. *RSC Advances* **2015**, *5*, 5131-5141. 10.1039/c4ra15865b
14. Pereira, C.; Pereira, A. M.; Rocha, M.; Freire, C.; Geraldes, C. F. G. C.: Architectured design of superparamagnetic Fe3O4 nanoparticles for application as MRI contrast agents: mastering size and magnetism for enhanced relaxivity. *Journal of Materials Chemistry B* **2015**, *3*, 6261-6273. 10.1039/c5tb00789e
15. Fernandes, C.; Pereira, C.; Fernandez-Garcia, M. P.; Pereira, A. M.; Guedes, A.; Fernandez-Pacheco, R.; Ibarra, A.; Ibarra, M. R.; Araujo, J. P.; Freire, C.: Tailored design of CoxMn1-xFe2O4 nanoferrites: a new route for dual control of size and magnetic properties. *Journal of Materials Chemistry C* **2014**, *2*, 5818-5828. 10.1039/c4tc00429a
16. Ravichandran, M.; Velumani, S.: Manganese ferrite nanocubes as an MRI contrast agent. *Materials Research Express* **2020**, *7*, 016107. 10.1088/2053-1591/ab66a4
17. Islam, K.; Haque, M.; Kumar, A.; Hoq, A.; Hyder, F.; Hoque, S. M.: Manganese Ferrite Nanoparticles (MnFe2O4): Size Dependence for Hyperthermia and Negative/Positive Contrast Enhancement in MRI. *Nanomaterials* **2020**, *10*, 2297. 10.3390/nano10112297
18. Gorgizadeh, M.; Behzadpour, N.; Salehi, F.; Daneshvar, F.; Vais, R. D.; Nazari-Vanani, R.; Azarpira, N.; Lotfi, M.; Sattarahmady, N.: A MnFe2O4/C nanocomposite as a novel theranostic agent in MRI, sonodynamic therapy and photothermal therapy of a melanoma cancer model. *Journal of Alloys and Compounds* **2020**, *816*, 152597. 10.1016/j.jallcom.2019.152597
19. Hu, J.; Dong, Y.-l.; Chen, X.-j.; Zhang, H.-j.; Zheng, J.-m.; Wang, Q.; Chen, X.-g.: A highly efficient catalyst: In situ growth of Au nanoparticles on graphene oxide–Fe3O4 nanocomposite support. *Chemical Engineering Journal* **2014**, *236*, 1-8. 10.1016/j.cej.2013.09.080
20. Zhang, W.; Liu, B.; Zhang, B.; Bian, G.; Qi, Y.; Yang, X.; Li, C.: Synthesis of monodisperse magnetic sandwiched gold nanoparticle as an easily recyclable catalyst with a protective polymer shell. *Colloids and Surfaces A: Physicochemical and Engineering Aspects* **2015**, *466*, 210-218. 10.1016/j.colsurfa.2014.11.055
21. Saire-Saire, S.; Barbosa, E. C. M.; Garcia, D.; Andrade, L. H.; Garcia-Segura, S.; Camargo, P. H. C.; Alarcon, H.: Green synthesis of Au decorated CoFe2O4 nanoparticles for catalytic reduction of 4-nitrophenol and dimethylphenylsilane oxidation. *RSC Advances* **2019**, *9*, 22116-22123. 10.1039/c9ra04222a
22. Silvestri, A.; Mondini, S.; Marelli, M.; Pifferi, V.; Falciola, L.; Ponti, A.; Ferretti, A. M.; Polito, L.: Synthesis of Water Dispersible and Catalytically Active Gold-Decorated Cobalt Ferrite Nanoparticles. *Langmuir* **2016**, *32*, 7117-7126. 10.1021/acs.langmuir.6b01266
23. Meng, X.; Li, B.; Ren, X.; Tan, L.; Huang, Z.; Tang, F.: One-pot gradient solvothermal synthesis of Au–Fe3O4 hybrid nanoparticles for magnetically recyclable catalytic applications. *Journal of Materials Chemistry A* **2013**, *1*, 10513-10517. 10.1039/c3ta12141k
24. Herzing, A. A.; Kiely, C. J.; Carley, A. F.; Landon, P.; Hutchings, G. J.: Identification of Active Gold Nanoclusters on Iron Oxide Supports for CO Oxidation. *Science* **2008**, *321*, 1331-1335. 10.1126/science.1159639
25. Fratila, R. M.; Mitchell, S. G.; del Pino, P.; Grazu, V.; de la Fuente, J. M.: Strategies for the Biofunctionalization of Gold and Iron Oxide Nanoparticles. *Langmuir* **2014**, *30*, 15057-15071. 10.1021/la5015658
26. Choi, J.; Park, S.; Stojanović, Z.; Han, H.-S.; Lee, J.; Seok, H. K.; Uskoković, D.; Lee, K. H.: Facile Solvothermal Preparation of Monodisperse Gold Nanoparticles and Their Engineered Assembly of Ferritin–Gold Nanoclusters. *Langmuir* **2013**, *29*, 15698-15703. 10.1021/la403888f
27. Ye, M.; Wei, Z.; Hu, F.; Wang, J.; Ge, G.; Hu, Z.; Shao, M.; Lee, S.-T.; Liu, J.: Fast assembling microarrays of superparamagnetic Fe3O4@Au nanoparticle clusters as reproducible substrates for surface-enhanced Raman scattering. *Nanoscale* **2015**, *7*, 13427-13437. 10.1039/c5nr02491a
28. Saikova, S.; Pavlikov, A.; Trofimova, T.; Mikhlin, Y.; Karpov, D.; Asanova, A.; Grigoriev, Y.; Volochaev, M.; Samoilo, A.; Zharkov, S.; Velikanov, D.: Hybrid Nanoparticles Based on Cobalt Ferrite and Gold: Preparation and Characterization. *Metals* **2021**, *11*, 705. 10.3390/met11050705

29. Binaymotlagh, R.; Hajareh Haghighi, F.; Aboutalebi, F.; Mirahmadi-Zare, S. Z.; Hadadzadeh, H.; Nasr-Esfahani, M.-H.: Selective chemotherapy and imaging of colorectal and breast cancer cells by a modified MUC-1 aptamer conjugated to a poly(ethylene glycol)-dimethacrylate coated Fe3O4–AuNCs nanocomposite. *New Journal of Chemistry* **2019**, *43*, 238-248. 10.1039/c8nj04236e
30. Le Guével, X.; Prinz, E.-M.; Müller, R.; Hempelmann, R.; Schneider, M.: Synthesis and characterization of superparamagnetic nanoparticles coated with fluorescent gold nanoclusters. *Journal of Nanoparticle Research* **2012**, *14*, 727. 10.1007/s11051-012-0727-6
31. Huang, C.-L.; Hsieh, W.-J.; Lin, C.-W.; Yang, H.-W.; Wang, C.-K.: Multifunctional liposomal drug delivery with dual probes of magnetic resonance and fluorescence imaging. *Ceramics International* **2018**, *44*, 12442-12450. 10.1016/j.ceramint.2018.04.034
32. Guo, H.; Zhang, Y.; Liang, W.; Tai, F.; Dong, Q.; Zhang, R.; Yu, B.; Wong, W.-Y.: An inorganic magnetic fluorescent nanoprobe with favorable biocompatibility for dual-modality bioimaging and drug delivery. *Journal of Inorganic Biochemistry* **2019**, *192*, 72-81. 10.1016/j.jinorgbio.2018.12.002
33. Wang, C.; Yao, Y.; Song, Q.: Gold nanoclusters decorated with magnetic iron oxide nanoparticles for potential multimodal optical/magnetic resonance imaging. *Journal of Materials Chemistry C* **2015**, *3*, 5910-5917. 10.1039/c5tc00290g
34. Xu, Y.; Palchoudhury, S.; Qin, Y.; Macher, T.; Bao, Y.: Make Conjugation Simple: A Facile Approach to Integrated Nanostructures. *Langmuir* **2012**, *28*, 8767-8772. 10.1021/la301200g
35. Luo, S.; Liu, Y.; Rao, H.; Wang, Y.; Wang, X.: Fluorescence and magnetic nanocomposite Fe3O4@SiO2@Au MNPs as peroxidase mimetics for glucose detection. *Analytical Biochemistry* **2017**, *538*, 26-33. 10.1016/j.ab.2017.09.006
36. Kim, D.; Lee, B.: Fluorescence detection of bisphenol A in aqueous solution using magnetite core-shell material with gold nanoclusters prepared by molecular imprinting technique. *Korean J. Chem. Eng.* **2019**, *36*, 1509-1517. 10.1007/s11814-019-0342-7
37. Ribeiro, T.; Rodrigues, A. S.; Calderon, S.; Fidalgo, A.; Gonçalves, J. L. M.; André, V.; Teresa Duarte, M.; Ferreira, P. J.; Farinha, J. P. S.; Baleizão, C.: Silica nanocarriers with user-defined precise diameters by controlled template self-assembly. *Journal of Colloid and Interface Science* **2020**, *561*, 609-619. 10.1016/j.jcis.2019.11.036
38. Calderon V, S.; Ribeiro, T.; Farinha, J. P. S.; Baleizão, C.; Ferreira, P. J.: On the Structure of Amorphous Mesoporous Silica Nanoparticles by Aberration-Corrected STEM. *Small* **2018**, *14*, 1802180. 10.1002/smll.201802180
39. Gonçalves, J. L. M.; J. Castanheira, E.; P. C. Alves, S.; Baleizão, C.; Farinha, J. P.: Grafting with RAFT—gRAFT Strategies to Prepare Hybrid Nanocarriers with Core-shell Architecture. *Polymers* **2020**, *12*, 2175. 10.3390/polym12102175
40. Ribeiro, T.; Coutinho, E.; Rodrigues, A. S.; Baleizão, C.; Farinha, J. P. S.: Hybrid mesoporous silica nanocarriers with thermovalve-regulated controlled release. *Nanoscale* **2017**, *9*, 13485-13494. 10.1039/C7NR03395H
41. Tavares, M. T.; Oliveira, M. B.; Gaspar, V. M.; Mano, J. F.; S. Farinha, J. P.; Baleizão, C.: Efficient Single-Dose Induction of Osteogenic Differentiation of Stem Cells Using Multi-Bioactive Hybrid Nanocarriers. **2020**, *4*, 2000123. 10.1002/adbi.202000123
42. Gonçalves, J. L. M.; Lopes, A. B. C.; Baleizão, C.; Farinha, J. P. S.: Mesoporous Silica Nanoparticles Modified inside and out for ON:OFF pH-Modulated Cargo Release. *Pharmaceutics* **2021**, *13*, 716. 10.3390/pharmaceutics13050716
43. Gonçalves, J. L. M.; Crucho, C. I. C.; Alves, S. P. C.; Baleizão, C.; Farinha, J. P. S.: Hybrid Mesoporous Nanoparticles for pH-Actuated Controlled Release. *Nanomaterials* **2019**, *9*, 483. 10.3390/nano9030483
44. Baleizão, C.; Farinha, J. P. S.: Hybrid smart mesoporous silica nanoparticles for theranostics. *Nanomedicine* **2015**, *10*, 2311-2314. 10.2217/nnm.15.102
45. Saroj, S.; Rajput, S. J.: Composite smart mesoporous silica nanoparticles as promising therapeutic and diagnostic candidates: Recent trends and applications. *Journal of Drug Delivery Science and Technology* **2018**, *44*, 349-365. 10.1016/j.jddst.2018.01.014
46. Liu, D.; Wang, J.; Zhang, Y.; Liu, J.; Li, H.; Zhou, L.; Wu, S.; Gao, X.: Preparation of core–shell structured Au@SiO2 nanocomposite catalyst with Au core size below 2 nm without high-temperature calcination procedure. *Journal of Materials Science* **2018**, *53*, 8086-8097. 10.1007/s10853-018-2085-y

47. Yan, W.; Chen, B.; Mahurin, S. M.; Hagaman, E. W.; Dai, S.; Overbury, S. H.: Surface Sol–Gel Modification of Mesoporous Silica Materials with TiO2 for the Assembly of Ultrasmall Gold Nanoparticles. *The Journal of Physical Chemistry B* **2004**, *108*, 2793-2796. 10.1021/jp037713z
48. Liu, Y.; Tsunoyama, H.; Akita, T.; Tsukuda, T.: Preparation of ~1 nm Gold Clusters Confined within Mesoporous Silica and Microwave-Assisted Catalytic Application for Alcohol Oxidation. *The Journal of Physical Chemistry C* **2009**, *113*, 13457-13461. 10.1021/jp904700p
49. Casteleiro, B.; Martinho, J. M. G.; Farinha, J. P. S.: Encapsulation of gold nanoclusters: stabilization and more. *Nanoscale* **2021**, *13*, 17199-17217. 10.1039/d1nr04939a
50. He, F.; Yang, G.; Yang, P.; Yu, Y.; Lv, R.; Li, C.; Dai, Y.; Gai, S.; Lin, J.: A New Single 808 nm NIR Light-Induced Imaging-Guided Multifunctional Cancer Therapy Platform. *Adv. Funct. Mater.* **2015**, *25*, 3966-3976. 10.1002/adfm.201500464
51. Pereira, C.; Pereira, A. M.; Fernandes, C.; Rocha, M.; Mendes, R.; Fernández-García, M. P.; Guedes, A.; Tavares, P. B.; Grenèche, J.-M.; Araújo, J. P.; Freire, C.: Superparamagnetic MFe2O4 (M = Fe, Co, Mn) Nanoparticles: Tuning the Particle Size and Magnetic Properties through a Novel One-Step Coprecipitation Route. *Chemistry of Materials* **2012**, *24*, 1496-1504. 10.1021/cm300301c
52. Seybold, P. G.; Gouterman, M.: Porphyrins: XIII: Fluorescence spectra and quantum yields. *Journal of Molecular Spectroscopy* **1969**, *31*, 1-13. 10.1016/0022-2852(69)90335-X
53. Brust, M.; Walker, M.; Bethell, D.; Schiffrin, D. J.; Whyman, R.: Synthesis of thiol-derivatised gold nanoparticles in a two-phase Liquid-Liquid system. *Journal of the Chemical Society, Chemical Communications* **1994**, 801-802. 10.1039/c39940000801
54. Zhu, M.; Lanni, E.; Garg, N.; Bier, M. E.; Jin, R.: Kinetically Controlled, High-Yield Synthesis of Au25 Clusters. *Journal of the American Chemical Society* **2008**, *130*, 1138-1139. 10.1021/ja0782448
55. Huang, T.; Murray, R. W.: Visible luminescence of water-soluble monolayer- protected gold clusters. *Journal of Physical Chemistry B* **2001**, *105*, 12498-12502. 10.1021/jp0041151
56. Chen, L.-Y.; Wang, C.-W.; Yuan, Z.; Chang, H.-T.: Fluorescent Gold Nanoclusters: Recent Advances in Sensing and Imaging. *Analytical Chemistry* **2015**, *87*, 216-229. 10.1021/ac503636j
57. Casteleiro, B.; Ribeiro, T.; Mariz, I.; Martinho, J. M. G.; Farinha, J. P. S.: Encapsulation of gold nanoclusters by photo-initiated miniemulsion polymerization. *Colloids and Surfaces A: Physicochemical and Engineering Aspects* **2022**, 129410. 10.1016/j.colsurfa.2022.129410
58. Khan, Z.; Singh, T.; Hussain, J. I.; Hashmi, A. A.: Au(III)–CTAB reduction by ascorbic acid: Preparation and characterization of gold nanoparticles. *Colloids and Surfaces B: Biointerfaces* **2013**, *104*, 11-17. 10.1016/j.colsurfb.2012.11.017
59. Kubo, S.; Kosuge, K.: Salt-Induced Formation of Uniform Fiberlike SBA-15 Mesoporous Silica Particles and Application to Toluene Adsorption. *Langmuir* **2007**, *23*, 11761-11768. 10.1021/la701556y
60. Pereira, C.; Pereira, A. M.; Quaresma, P.; Tavares, P. B.; Pereira, E.; Araújo, J. P.; Freire, C.: Superparamagnetic γ-Fe2O3@SiO2 nanoparticles: a novel support for the immobilization of [VO(acac)2]. *Dalton Transactions* **2010**, *39*, 2842-2854. 10.1039/b920853d
61. Fidalgo, A.; Ilharco, L. M.: The defect structure of sol–gel-derived silica/polytetrahydrofuran hybrid films by FTIR. *Journal of Non-Crystalline Solids* **2001**, *283*, 144-154. 10.1016/S0022-3093(01)00418-5
62. Dupuis, R.; Pellenq, R.; Champenois, J.-B.; Poulesquen, A.: Dissociation Mechanisms of Dissolved Alkali Silicates in Sodium Hydroxide. *The Journal of Physical Chemistry C* **2020**, *124*, 8288-8294. 10.1021/acs.jpcc.0c01495
63. Safdar, M. H.; Hasan, H.; Anees, M.; Hussain, Z.: FOLIC ACID-CONJUGATED DOXORUBICIN-LOADED PHOTOSENSITIZING MANGANESE FERRITE NANOPARTICLES: SYNTHESIS, CHARACTERIZATION AND ANTICANCER ACTIVITY AGAINST HUMAN CERVICAL CARCINOMA CELL LINE (HELA). *International Journal of Pharmacy and Pharmaceutical Sciences* **2017**, *9*, 60-67. 10.22159/ijpps.2017v9i5.17261
64. León-Félix, L.; Chaker, J.; Parise, M.; Coaquira, J. A. H.; De Los Santos Valladares, L.; Bustamante, A.; Garg, V. K.; Oliveira, A. C.; Morais, P. C.: Synthesis and characterization of uncoated and gold-coated magnetite nanoparticles. *Hyperfine Interactions* **2014**, *224*, 179-188. 10.1007/s10751-013-0857-y
65. Banerjee, S.; Raja, S. O.; Sardar, M.; Gayathri, N.; Ghosh, B.; Dasgupta, A.: Iron oxide nanoparticles coated with gold: Enhanced magnetic moment due to interfacial effects. *Journal of Applied Physics* **2011**, *109*, 123902. 10.1063/1.3596760

66. Wang, L.; Park, H.-Y.; Lim, S. I. I.; Schadt, M. J.; Mott, D.; Luo, J.; Wang, X.; Zhong, C.-J.: Core@shell nanomaterials: gold-coated magnetic oxide nanoparticles. *Journal of Materials Chemistry* **2008**, *18*, 2629-2635. 10.1039/b719096d
67. Khan, G. G.; Sarkar, D.; Singh, A. K.; Mandal, K.: Enhanced band gap emission and ferromagnetism of Au nanoparticle decorated α-Fe2O3 nanowires due to surface plasmon and interfacial effects. *RSC Advances* **2013**, *3*, 1722-1727. 10.1039/c2ra22578f
68. Agrachev, M.; Antonello, S.; Dainese, T.; Ruzzi, M.; Zoleo, A.; Aprà, E.; Govind, N.; Fortunelli, A.; Sementa, L.; Maran, F.: Magnetic Ordering in Gold Nanoclusters. *ACS Omega* **2017**, *2*, 2607-2617. 10.1021/acsomega.7b00472
69. Tuboltsev, V.; Savin, A.; Pirojenko, A.; Räisänen, J.: Magnetism in Nanocrystalline Gold. *ACS Nano* **2013**, *7*, 6691-6699. 10.1021/nn401914b
70. Krishna, K. S.; Tarakeshwar, P.; Mujica, V.; Kumar, C. S. S. R.: Chemically Induced Magnetism in Atomically Precise Gold Clusters. *Small* **2014**, *10*, 907-911. 10.1002/smll.201302393
71. Pereira, A. M.; Pereira, C.; Silva, A. S.; Schmool, D. S.; Freire, C.; Grenèche, J.-M.; Araújo, J. P.: Unravelling the effect of interparticle interactions and surface spin canting in γ-Fe2O3@SiO2 superparamagnetic nanoparticles. *Journal of Applied Physics* **2011**, *109*, 114319. 10.1063/1.3583652
72. Huang, R.; Tang, T.: Assembly of Magnetic Nano-Fe3O4@GSH-Au NCs Core–Shell Microspheres for the Visualization of Latent Fingerprints. *Nano* **2018**, *13*, 1850128. 10.1142/s179329201850128x
73. Xiao, X.; Yang, H.; Jiang, P.; Chen, Z.; Ji, C.; Nie, L.: Multi-Functional Fe3O4@mSiO2-AuNCs Composite Nanoparticles Used as Drug Delivery System. *Journal of Biomedical Nanotechnology* **2017**, *13*, 1292-1299. 10.1166/jbn.2017.2417